Original Article | Neuroimaging and Head & Neck

eISSN 2005-8330
https://doi.org/10.3348/kjr.2022.0539
Korean J Radiol 2022;23(12):1281-1289

Korean Journal of Radiology
KJR

Development and Validation of MRI-Based Radiomics Models for Diagnosing Juvenile Myoclonic Epilepsy

Kyung Min Kim[1*], Heewon Hwang[2*], Beomseok Sohn[3], Kisung Park[3, 4], Kyunghwa Han[3], Sung Soo Ahn[3], Wonwoo Lee[5], Min Kyung Chu[1], Kyoung Heo[1], Seung-Koo Lee[3]

[1]Department of Neurology, Epilepsy Research Institute, Yonsei University College of Medicine, Seoul, Korea; [2]Department of Neurology, Wonju Severance Christian Hospital, Yonsei University Wonju College of Medicine, Wonju, Korea; [3]Department of Radiology, Severance Hospital, Research Institute of Radiological Science and Centre for Clinical Imaging Data Science, Yonsei University College of Medicine, Seoul, Korea; [4]Department of Mechanical Engineering, Pohang University of Science and Technology, Pohang, Korea; [5]Department of Neurology, Yongin Severance Hospital, Yonsei University Health System, Yongin, Korea

Objective: Radiomic modeling using multiple regions of interest in MRI of the brain to diagnose juvenile myoclonic epilepsy (JME) has not yet been investigated. This study aimed to develop and validate radiomics prediction models to distinguish patients with JME from healthy controls (HCs), and to evaluate the feasibility of a radiomics approach using MRI for diagnosing JME.

Materials and Methods: A total of 97 JME patients (25.6 ± 8.5 years; female, 45.5%) and 32 HCs (28.9 ± 11.4 years; female, 50.0%) were randomly split (7:3 ratio) into a training (n = 90) and a test set (n = 39) group. Radiomic features were extracted from 22 regions of interest in the brain using the T1-weighted MRI based on clinical evidence. Predictive models were trained using seven modeling methods, including a light gradient boosting machine, support vector classifier, random forest, logistic regression, extreme gradient boosting, gradient boosting machine, and decision tree, with radiomics features in the training set. The performance of the models was validated and compared to the test set. The model with the highest area under the receiver operating curve (AUROC) was chosen, and important features in the model were identified.

Results: The seven tested radiomics models, including light gradient boosting machine, support vector classifier, random forest, logistic regression, extreme gradient boosting, gradient boosting machine, and decision tree, showed AUROC values of 0.817, 0.807, 0.783, 0.779, 0.767, 0.762, and 0.672, respectively. The light gradient boosting machine with the highest AUROC, albeit without statistically significant differences from the other models in pairwise comparisons, had accuracy, precision, recall, and F1 scores of 0.795, 0.818, 0.931, and 0.871, respectively. Radiomic features, including the putamen and ventral diencephalon, were ranked as the most important for suggesting JME.

Conclusion: Radiomic models using MRI were able to differentiate JME from HCs.

Keywords: *Juvenile myoclonic epilepsy; Idiopathic generalized epilepsy; Radiomics; Texture analysis; Magnetic resonance imaging*

INTRODUCTION

Juvenile myoclonic epilepsy (JME) is a type of idiopathic generalized epilepsy (IGE) that presents with typical seizure types such as generalized tonic-clonic seizures, myoclonic jerks, and less frequently, absence seizures. JME is a major epilepsy syndrome, accounting for 5%–10% of all epilepsies and approximately 18% of idiopathic generalized epilepsies [1]. The clinical features of JME include an age of onset between 12 and 16 years, generalized spike-and-wave

Received: June 23, 2022 **Revised:** September 21, 2022 **Accepted:** September 26, 2022
*These authors contributed equally to this work.
Corresponding author: Beomseok Sohn, MD, Department of Radiology, Severance Hospital, Research Institute of Radiological Science and Centre for Clinical Imaging Data Science, Yonsei University College of Medicine, 50-1 Yonsei-ro, Seodaemun-gu, Seoul 03722, Korea.
• E-mail: beomseoksohn@yuhs.ac

complexes on the electroencephalogram (EEG), and normal routine brain MRI upon visual inspection [2].

Recently, advanced imaging analysis methods have revealed microstructural and functional brain abnormalities in JME patients. Computational MRI studies using voxel-based morphometry, diffusion tensor imaging, and functional MRI have shown changes in the cortical/subcortical volume and morphology, thalamocortical connectivity, and structural-functional correlations [3-5]. In contrast, previous studies have mainly focused on single regions of interest (ROI) (thalamus [6], putamen [7], corpus callosum [8], amygdala-hippocampus [9], and frontal cortex [10]) or single parameters (volume, morphology, probabilistic tractography connectivity, and blood-oxygen-level-dependent contrast).

Radiomics can provide information such as intensity distributions, spatial relationships, textural heterogeneity, and shape descriptors [11]. Radiomics aims to extract quantitative and ideally reproducible information, such as complex patterns that are difficult to recognize [12]. Thus, the radiomics methodology is thought to be useful in elucidating the complex pathogenic networks involved in epileptogenesis. Although recent studies have used radiomics in patients with epilepsy, radiomics studies in patients with JME are limited [13,14].

Therefore, this study aimed to develop and validate radiomics-based prediction models using routine conventional MRI to distinguish patients with JME from healthy controls (HCs). This study will be helpful in evaluating the feasibility of a radiomics approach using MRI for diagnosing JME.

MATERIALS AND METHODS

Patient Selection and Characteristics

A total of 103 consecutive JME patients (25.6 ± 8.5 years; female, 45.5%) were enrolled retrospectively, who visited the epilepsy clinic of Severance Hospital (tertiary care center) between January 2000 and December 2020. The initial diagnosis of patients with JME was reconfirmed by reviewing the medical records of the two institution's neurologists. JME was diagnosed based on the clinical and EEG features set by the International League Against Epilepsy [2]. All patients with JME had typical seizures, such as myoclonic jerks and generalized tonic-clonic seizures. Routine scalp EEG demonstrated generalized polyspikes or spike-and-wave complexes in all patients. The MRI interpretation records were normal. Two board-certified neuroradiologists (5-year and 11-year experiences) reviewed all the MRI data to confirm their previous reading, and no abnormal findings were discovered. Two patients with JME were excluded because of the poor image quality of the MRI examinations. For the control group, 45 healthy participants without a history of medical, neurological, or psychiatric disorders volunteered for brain MRI for research purposes in our hospital from June 2015 to June 2016. The MRI results of all the 45 HCs were normal. Subsequently, 32 HCs (28.9 ± 11.4 years; female, 50.0%) matching the age range and gender composition were finally chosen for study analysis.

This retrospective study was approved by the Institutional Review Board of Severance Hospital (IRB No. 4-2021-1196), and the requirement for informed consent was waived. All the procedures were performed in accordance with the Declaration of Helsinki.

Image Acquisition

All preoperative MRI scans were performed using a 3T MRI system with an eight-channel sensitivity-encoding head coil (Achieva or Ingenia, Philips Healthcare; TrioTim, Siemens). All images were submitted to two imaging experts for visual analysis. The detailed acquisition parameters are described in the Supplement.

Image Processing and Radiomic Feature Extraction

During image processing and feature extraction, the status of the patients (JME vs. HCs) was blinded. Pre-processing of the images was performed to standardize the data analysis across patients. The FreeSurfer 6.0.0 software (https://surfer.nmr.mgh.harvard.edu) was used to obtain subject-specific masks of brain regions. This procedure involves motion correction of T1-weighted images, removal of non-brain tissue [15], automatic Talairach transformation, segmentation of subcortical white matter and deep gray matter structures [16], intensity normalization, tesselation of the gray matter/white matter boundary [17], automated topology correction, and surface deformation following intensity gradients [18]. The FreeSurfer automatically segments multiple brain structures. During auto-segmentation, four patients with JME were excluded because of segmentation errors. From multiple segmentations of brain structures, 22 ROI masks were selected based on clinical evidence from previous JME imaging research: bilateral cerebral white matter [19,20], bilateral thalamus [7,21], bilateral caudate [22,23],

https://doi.org/10.3348/kjr.2022.0539

Korean Journal of Radiology
KJR

bilateral putamen [7,24], bilateral globus pallidus [25], bilateral hippocampus [26,27], bilateral amygdala [9,28], bilateral ventral diencephalon [29,30], brainstem [31], and corpus callosum (anterior, mid-anterior, central, mid-posterior, and posterior) [32,33]. Their clinical relevance has been established through a review of published studies [34,35]. Subsequently, the T1-weighted images were re-sampled to an identical spatial resolution of 1 x 1 x 1 mm. A board-certified neuroradiologist inspected all the images and masks to ensure accuracy. No modifications were made to maintain a fully automated segmentation pipeline. These images were subjected to N4 bias correction to remove low-frequency intensity and non-uniformity. Subsequently, z-score image normalization was performed. Subsequently, radiomic features were extracted from the masks on T1WI using PyRadiomics (http://www.radiomics.io/pyradiomics.html) with a bin count of 32, including shape, first order, grey level co-occurrence matrix, grey level run-length matrix, grey-level size zone matrix, neighboring grey tone difference matrix, and grey level dependence matrix [36].

Machine Learning and Statistical Analysis

A random stratified split was performed to divide the 129 patients into training and test sets (7:3 ratio). The stratification factor was the diagnosis of the patients. To achieve a high-performing model, a grid search was conducted on the following machine learning methods: 1) logistic regression, 2) support vector classifier (SVC), 3) decision tree, 4) random forest, 5) gradient boosting machine (GBM), 6) LightGBM, and 7) extreme gradient boosting (XGBoost). A detailed description is provided in the Supplement. Radiomic feature values were z-normalized for logistic regression and the SVC model, whereas the original feature values were used for the tree-based models. If the feature reduction step was not built-in in the machine learning method, the LASSO feature reduction was applied first. The models were trained using the training sets, and a hyperparameter tuning was performed. Hyperparameter tuning was done by a 5-fold cross-validation in the training set. Efforts were made to adhere to the radiomics quality score system and transparent reporting of a multivariable prediction model for the individual prognosis OR diagnosis (TRIPOD) initiative as much as possible. However, as the HC cohorts were age- and sex-matched to the JME cohort, there were no clinically significant differences in age and sex between the JME and HC groups. Therefore, a multivariable analysis with those non-radiomics features was not performed [37,38].

The model employs weighted scaling and the synthetic minority oversampling technique (SMOTE) for further performance improvement [39]. The patient was blinded during the development and tuning of the models. The performance of each fine-tuned model was calculated using the test set, including accuracy, precision, recall, F1 score, and area under the receiver operating characteristics curve (AUROC). For a cut-off value of 0.5, the median probability value was chosen. The AUROC was compared between the model with the highest AUROC and each other in a pairwise manner using the Delong's method.

To examine which features played an important role in the final prediction, the mean absolute Shapley value for each of the selected input features was calculated using the Shapley additive explanations (SHAP) algorithm in the model with the highest AUROC [40].

Reconfirm the Performance of Selected Machine Learning Method and Important Features

Considering the repeatability of the machine learning method and the robustness of the selected features, reconfirmation was performed using the machine learning technique with the highest AUROC. The identical training and test sets were used. The SMOTE and MinMaxScaler were used for feature pre-processing. The SelectKBest approach's f-classification and mutual information methods were used to select the features. An odd number of features—one to 39, were chosen. Finally, a total of forty models were constructed. In the test set, the AUROC of the 40 models were calculated. According to their anatomical structures, the number of chosen features was tallied for each of the 40 models.

All processes up to this point were carried out using the Python 3 (Python Software Foundation) with the Scikit-learn library v0.21.2, and the R software (version 3.5.1; R Foundation for Statistical Computing). $p < 0.05$ was considered to indicate a statistically significant difference; p values were two-sided.

RESULTS

Finally, 97 patients with JME and 32 HCs were recruited for this study. The median age of onset and mean duration of JME were 14 years (range, 7–22 years) and 7 years (range, 1–42 years), respectively. 27 patients were drug-naïve, and 70 were taking antiseizure medications. The JME and HC

 https://doi.org/10.3348/kjr.2022.0539

groups had similar mean ages (mean ± SD; JME = 25.6 ± 8.5; HC = 28.9 ± 11.4; p = 0.136) and gender composition (female %; JME = 45.4%; HC = 50.0%, p = 0.648). After a random stratified split, the 129 subjects were divided into either a training set group (n = 90) or a test set group (n = 39); their characteristics are shown in Table 1. There were no statistically significant differences between the training and test sets.

For all the 129 patients, fully automated segmentation of deep brain structures was successfully achieved using the FreeSurfer software. A total of 2354 radiomic features were extracted from each patient using the PyRadiomics pipeline. The flow of this investigation is shown in Figure 1. The seven radiomics models, LightGBM, SVC, random forest, logistic regression, XGBoost, GBM, and decision tree, showed AUROC values of 0.817, 0.807, 0.783, 0.779, 0.767, 0.762, and 0.672, respectively, in the test set (Fig. 2), and their further performance results are shown in Table 2. The LightGBM model showed the highest AUROC, although it did not show a statistically significant difference from other models (Table 2). The performance of the LightGBM model was 79.5% in accuracy, 80.0% in precision, 96.6% in recall, and 87.5% in the F1 score.

The mean absolute Shapley value for each feature of the model was calculated to assess feature importance. Two features from the putamen and one from the ventral diencephalon were ranked as the most important (Fig. 3). High values of dependence non-uniformity and zone percentage from the right and left putamen, respectively, could successfully predict JME. Conversely, low values of large-area high gray-level emphasis from the right ventral diencephalon were important for predicting the absence of JME in HCs.

Forty LightGBM models were produced as a consequence

Table 1. Clinical Characteristics of the Training and Test Sets

	Training Set (n = 90)	Test Set (n = 39)	*P*
Age, years	27.3 ± 10.6	24.5 ± 7.7	0.114
Sex			0.661
Male	47 (52.2)	22 (56.4)	
Female	43 (47.8)	17 (43.6)	
Status			0.885
JME	68 (75.6)	29 (74.4)	
HC	22 (24.4)	10 (25.6)	

Age indicates the mean ± standard deviation. Other data are presented as the number of patients with % in parentheses. HC = healthy control, JME = juvenile myoclonic epilepsy

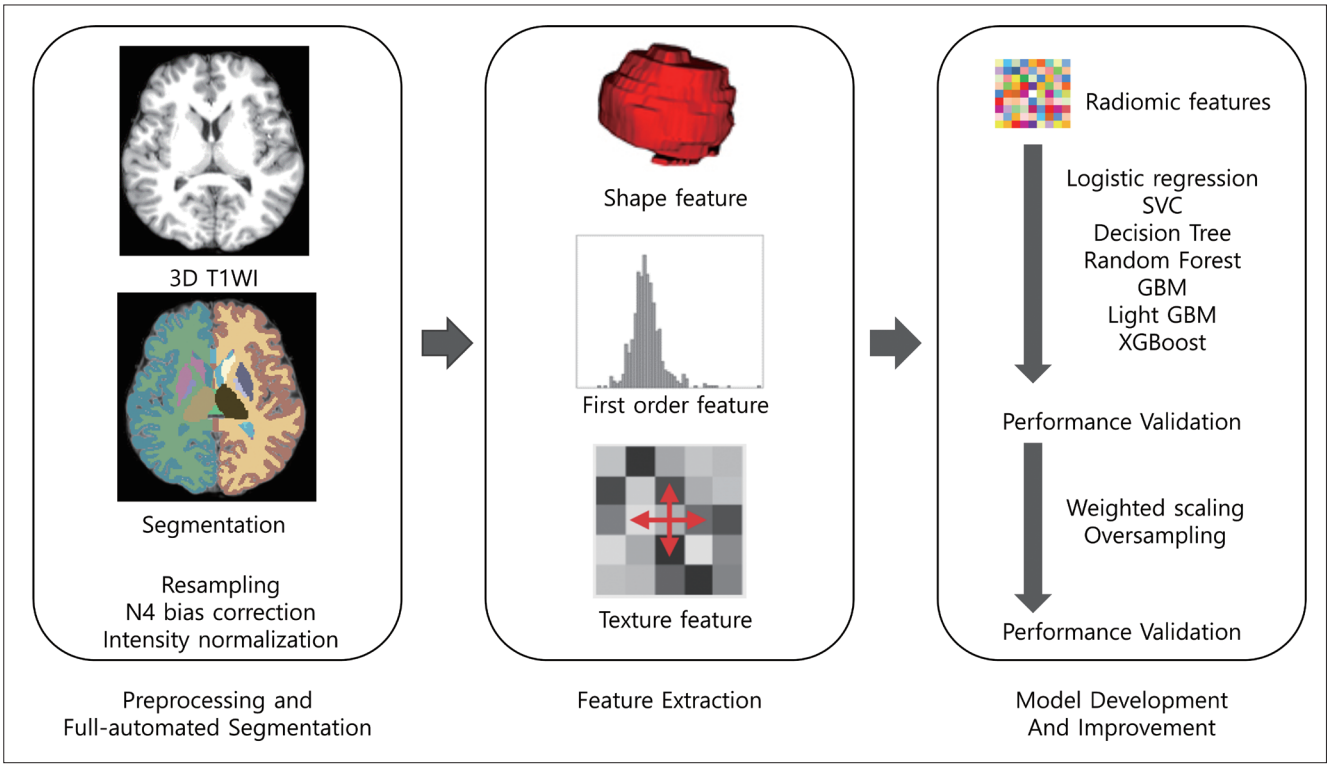

Fig. 1. Flowchart of image processing, radiomics feature extraction, machining learning model development, and performance validation. GBM = gradient boosting classifier, LightGBM = light gradient boosting machine, SVC = support vector classifier, T1WI = T1 weighted image, XGBoost = extra gradient boost

https://doi.org/10.3348/kjr.2022.0539

Korean Journal of Radiology
KJR

of reconfirmation. As a result of the SelectKBest methodology, each model selected a specific number of features (ranging from one to 39). From the 40 models in the test set, the average AUROC value was 0.795 (range 0.714–0.831). Among the 800 selected features from the 40 models, the putamen contributed 507 features, followed by the thalamus (n = 135), ventral diencephalon (n = 101), and caudate (n = 36).

DISCUSSION

The main findings of this study were as follows: 1) radiomics models, including multiple ROIs, may have the potential to discern patients with JME from HCs, and 2) the putamen has important radiomics features for predicting JME.

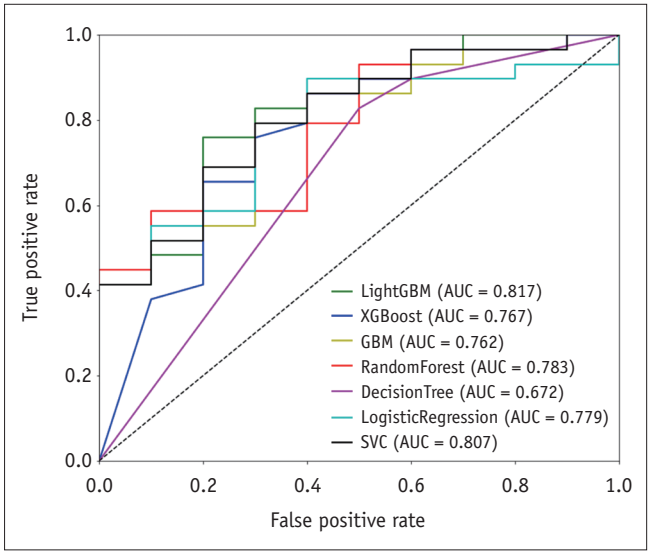

Fig. 2. ROC curves of all models in the test set. AUC = area under the curve, GBM = gradient boosting machine, LightGBM = light gradient boosting machine, ROC = receiver operating characteristic, SVC = support vector classifier, XGBoost = extra gradient boost

Early diagnosis of JME is pivotal for a favorable prognosis [41]. However, JME has often not been recognized by clinicians, and until now, its diagnosis has mainly been based on clinical and characteristic EEG features. Several quantitative MRI studies using voxel-based morphometry (VBM) have been published. Many studies have revealed thalamus and cortex anomalies in patients with JME compared with HCs [30,42,43]. The radiomics approach could have a similar advantage to VBM using the VBM software. It could also provide robust segmentation and volumetric analysis, as well as textural analysis. In addition, several studies using surface-based morphometry (SBM) have shown cortical thickness changes in the multifocal cortex [44,45]. The SBM can analyze the gyral curvature or connectivity of multiple gyri and sulci [46]. However, our approach does not reflect the different characteristics of the cortex. Instead of cortex parcellation, we focused more on segmentation and holistic shape, first-order, and texture feature analysis of the subcortical deep gray matter. Another advantage of the radiomic approach is that it can include the white matter analysis using multiple ROI. Many previous studies have investigated white matter changes using various methods [19,20,47]. Some studies have utilized neural networks. Recently, a study reported that advanced diffusion MRI and convolutional neural networks can detect JME with reliable accuracy [48]. Our radiomics models showed comparable performance to conventional T1 weighted MRI in differentiating patients with JME from HCs. In light of the increasing amount of JME imaging research, it is necessary to create a model that can use such data by combining multiple ROIs across several brain structures, which was the aim of this study. The tree-based machine learning method LightGBM showed the highest AUCs in this study. The tree-based machine learning methods are

Table 2. The Performances of the Final Models in the Test Set

	Final Model				AUROC (95% CI)	*P**
	Accuracy	Precision	Recall	F1 Score		
LightGBM	0.795 (31/39)	0.818 (27/33)	0.931 (27/29)	0.871	0.817 (0.665–0.970)	Reference
SVC	0.795 (31/39)	0.862 (25/29)	0.862 (25/26)	0.862	0.807 (0.654–0.959)	0.460
Random forest	0.769 (30/39)	0.778 (28/36)	0.966 (28/29)	0.862	0.783 (0.623–0.942)	0.446
Logistic regression	0.769 (30/39)	0.857 (24/28)	0.828 (24/29)	0.842	0.779 (0.622–0.937)	0.575
XGBoost	0.795 (31/39)	0.800 (28/35)	0.966 (28/29)	0.875	0.767 (0.580–0.954)	0.103
GBM	0.769 (30/39)	0.813 (26/32)	0.897 (26/29)	0.852	0.762 (0.597–0.927)	0.561
Decision tree	0.769 (30/39)	0.813 (26/32)	0.897 (26/29)	0.852	0.672 (0.490–0.854)	0.848

A cut-off value of 0.5, the median of the probability, was used to obtain performance metrics. *p value was used for pairwise comparison of AUROC values between LightGBM and each other model using Delong's method. AUROC = area under the receiver operating characteristic curve, CI = confidence interval, GBM = gradient boosting classifier, LightGBM = light gradient boosting machine, SVC = support vector classifier, XGBoost = extra gradient boost

https://doi.org/10.3348/kjr.2022.0539

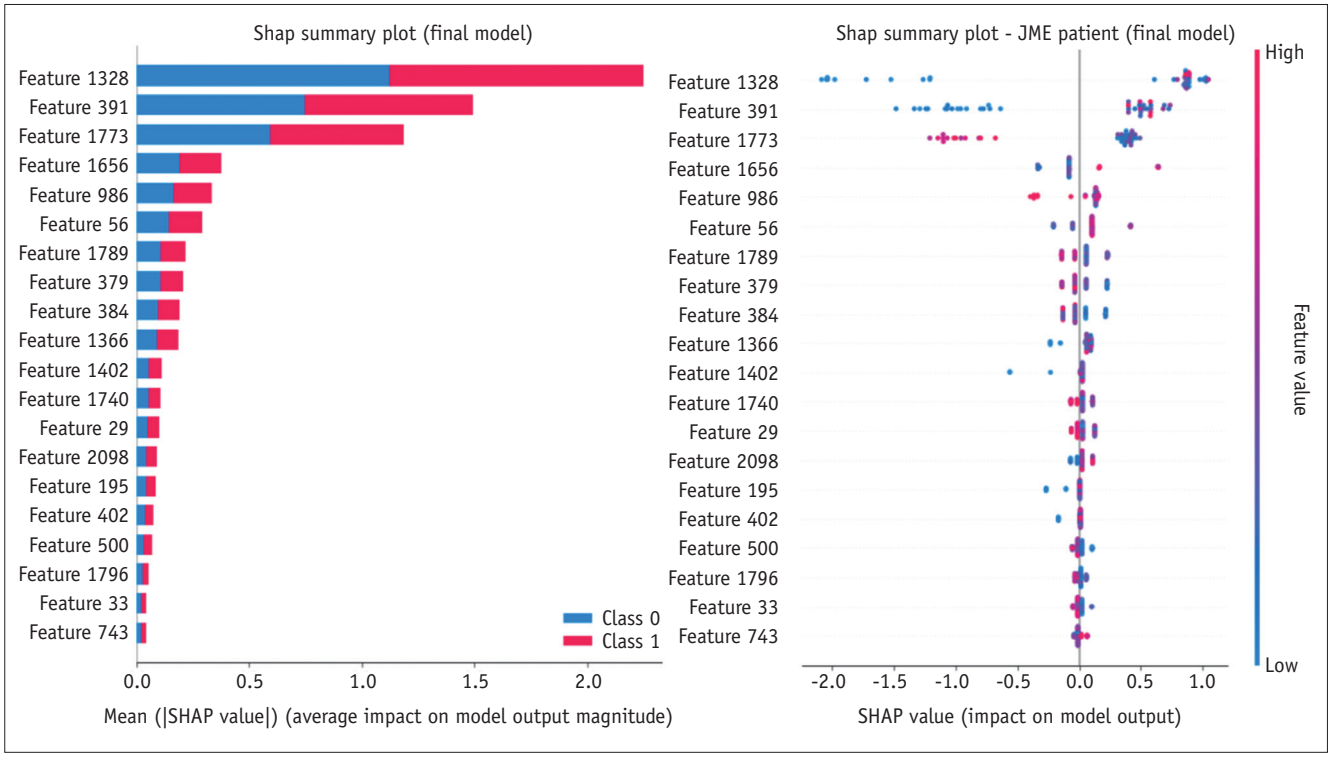

Fig. 3. The feature importance according to the mean absolute SHAP value for the prediction of JME in the LightGBM model from the test set. Feature 1328 (right putamen dependence non-uniformity normalized), feature 391 (left putamen zone percentage), and feature 1773 (right ventral diencephalon large area high gray level emphasis) were ranked as the highest three in importance. Feature 1328: right putamen (dependence non-uniformity normalized), feature 391: left putamen (zone percentage), feature 1773: right ventral diencephalon (large-area high-gray-level emphasis), feature 1656: right amygdala (large dependence low gray level), feature 986: WM, right side (correlation), feature 56: WM, left side (gray level non-uniformity), feature 1789: right ventral diencephalon (long-run high gray level emphasis), feature 379: left putamen (gray level variance), feature 384: left putamen (low gray level zone emphasis), feature 1366: right putamen (run length non-uniformity normalized). JME = juvenile myoclonic epilepsy, LightGBM = light gradient boosting machine, SHAP = shapley additive explanation, WM = white matter

relatively easy to understand and do not require feature scaling such as standardization or normalization [49]. In addition, the LightGBM has a relatively high learning speed. Therefore, the LightGBM method can be effectively used in radiomics-based machine-learning studies. Given that the protocol employed in this study showed relatively high predictive power for JME, the described methods should be considered highly valid for future radiomics research on patients with epilepsy.

In this study, the SHAP values of the model were investigated. The mean absolute Shapley value has been introduced here to create an explainable radiomics model and solve its notorious "black box" nature [40]. In this study, the putamen and ventral diencephalon had high SHAP values in the LightGBM model, suggesting that they are likely to have abnormalities in the brains of patients with JME. In addition, putamen-derived features were frequently selected by the reconfirmation process. Among the 40 models, the putamen contributed the most (507/800, 63.4%). The putamen has been shown to have microstructural and macrostructural defects in previous JME studies [7], and has been implicated in the pathophysiology of JME as a site of decreased dopamine receptor binding [50]. The ventral diencephalon is an unfamiliar anatomical structure in the human brain. Ventral diencephalon masks were generated using Freesurfer's auto-segmentation. Given the location of the ventral diencephalon mask, it covers the ventral posterior thalamus, which is related to JME (Supplementary Fig. 1) [3,51]. Nevertheless, our full auto-segmentation pipeline using open-source software is preferred over the semi-auto-segmentation or manual segmentation because it is a reproducible and reliable method that is unaffected by inter- or intra-rater differences. Furthermore, the time-consuming laborious nature of mapping the ROI is a fundamental downside of the radiomic technique, which can be significantly diminished by auto-segmentation. On the other hand, the FreeSurfer's auto-segmentation is free from laborious ROI

https://doi.org/10.3348/kjr.2022.0539

Korean Journal of Radiology
KJR

mapping; however, it is still a time-consuming process. We hope that this aspect will be alleviated in future studies, for example, by adopting Fastsurfer or other deep learning-based segmentation programs.

This study had several limitations. First, owing to the low prevalence of JME, this investigation was conducted with a limited sample size at a single institution. Further research with a larger sample size at multiple centers is needed for external validation. An external validation would be beneficial for assessing the reproducibility and optimizing the model. To prevent overfitting and validate the model, an independent test set was used as a feasible and practical method in this study. In addition, the same machine learning method was trained several times with varying quantities of features to confirm that there was no significant degradation in performance. The primary purpose of this study was to evaluate the feasibility of a radiomics approach using brain MRI for the diagnosis of JME. An external validation has not yet been performed using the JME radiomics. Second, it was impossible to obtain three-dimensional fluid-attenuated inversion recovery (3D-FLAIR) images of some patients; therefore, the study was conducted using only the T1-weighted images. Future studies are needed to achieve increased accuracy by adding FLAIR 3D images or other multiparametric MRI sequences. Third, this study did not exclude the effects of disease exposure and treatment. However, a wide range of disease durations and treatment exposures may reflect the real clinical settings. More number of patients are needed to confirm the statistical significance of the wide range of epilepsy durations. Finally, radiomic features from 22 distinct ROIs were derived, and the results were sensitive to feature clustering. Multi-collinearity is a major issue, because it introduces bias when calculating the regression coefficient of each feature. However, machine-learning studies often focus on the predictive power of all features rather than testing each variable individually. Nevertheless, further research is required to overcome this correlation issue.

This study had several strengths. First, this study developed and validated a diagnostic model for JME with the radiomics features of routine conventional MRI. JME is a major epileptic syndrome within IGE, but is often underdiagnosed [52]. The role of MRI as a diagnostic tool is limited because it shows visually normal MRI in JME. However, the MRI prediction model proposed in this study can improve clinical suspicion and prognosis by reducing the duration of unsuccessful treatment [41]. Second, by creating a model using multiple ROIs, this study comprehensively evaluated the brain structures implicated in previous studies as likely to have structural and functional abnormalities in the JME. Finally, these results showed some consistency with the results of several previous investigations, thus suggesting the validity of our methods for application in subsequent studies.

In conclusion, radiomics models using MRI were able to differentiate JME from HCs and may be feasible as a method to diagnose JME. Therefore, further studies are warranted.

Supplement

The Supplement is available with this article at https://doi.org/10.3348/kjr.2022.0539.

Availability of Data and Material

The datasets generated or analyzed during the study are available from the corresponding author on reasonable request.

Conflicts of Interest

Kyunghwa Han who is on the editorial board of the *Korean Journal of Radiology* was not involved in the editorial evaluation or decision to publish this article. All remaining authors have declared no conflicts of interest.

Author Contributions

Conceptualization: Kyung Min Kim, Beomseok Sohn. Data curation: Kyung Min Kim, Heewon Hwang. Formal analysis: Kyung Min Kim, Heewon Hwang, Beomseok Sohn. Funding acquisition: Beomseok Sohn. Investigation: Kyung Min Kim, Heewon Hwang, Beomseok Sohn. Methodology: Kyunghwa Han, Kisung Park, Beomseok Sohn. Project administration: Beomseok Sohn. Resources: Kyung Min Kim, Heewon Hwang, Wonwoo Lee, Kyoung Heo. Software: Kisung Park, Beomseok Sohn. Supervision: Sung Soo Ahn, Wonwoo Lee, Min Kyung Chu, Kyoung Heo, Seung-Koo Lee. Validation: Beomseok Sohn, Kyunghwa Han. Visualization: Kyunghwa Han, Beomseok Sohn, Kisung Park. Writing—original draft: Kyung Min Kim, Heewon Hwang. Writing—review & editing: all authos.

ORCID iDs

Kyung Min Kim
https://orcid.org/0000-0002-0261-1687

Heewon Hwang
https://orcid.org/0000-0002-0782-6724
Beomseok Sohn
https://orcid.org/0000-0002-6765-8056
Kisung Park
https://orcid.org/0000-0002-7447-4247
Kyunghwa Han
https://orcid.org/0000-0002-5687-7237
Sung Soo Ahn
https://orcid.org/0000-0002-0503-5558
Wonwoo Lee
https://orcid.org/0000-0002-0907-4212
Min Kyung Chu
https://orcid.org/0000-0001-6221-1346
Kyoung Heo
https://orcid.org/0000-0002-0790-9837
Seung-Koo Lee
https://orcid.org/0000-0001-5646-4072

Funding Statement
None

REFERENCES

1. Camfield CS, Striano P, Camfield PR. Epidemiology of juvenile myoclonic epilepsy. *Epilepsy Behav* 2013;28 Suppl 1:S15-S17
2. No authors listed. Proposal for revised classification of epilepsies and epileptic syndromes. Commission on classification and terminology of the international league against epilepsy. *Epilepsia* 1989;30:389-399
3. Cao B, Tang Y, Li J, Zhang X, Shang HF, Zhou D. A meta-analysis of voxel-based morphometry studies on gray matter volume alteration in juvenile myoclonic epilepsy. *Epilepsy Res* 2013;106:370-377
4. O'Muircheartaigh J, Vollmar C, Barker GJ, Kumari V, Symms MR, Thompson P, et al. Abnormal thalamocortical structural and functional connectivity in juvenile myoclonic epilepsy. *Brain* 2012;135(Pt 12):3635-3644
5. Roebling R, Scheerer N, Uttner I, Gruber O, Kraft E, Lerche H. Evaluation of cognition, structural, and functional MRI in juvenile myoclonic epilepsy. *Epilepsia* 2009;50:2456-2465
6. de Oliveira MS, Betting LE, Mory SB, Cendes F, Castellano G. Texture analysis of magnetic resonance images of patients with juvenile myoclonic epilepsy. *Epilepsy Behav* 2013;27:22-28
7. Keller SS, Ahrens T, Mohammadi S, Möddel G, Kugel H, Ringelstein EB, et al. Microstructural and volumetric abnormalities of the putamen in juvenile myoclonic epilepsy. *Epilepsia* 2011;52:1715-1724
8. Filho GM, Jackowski AP, Lin K, Silva I, Guaranha MSB, Guilhoto LM, et al. The integrity of corpus callosum and cluster B personality disorders: a quantitative MRI study in juvenile myoclonic epilepsy. *Prog Neuropsychopharmacol Biol Psychiatry* 2010;34:516-521
9. Lee DA, Ko J, Lee HJ, Kim HC, Park BS, Park S, et al. Alterations of the intrinsic amygdala-hippocampal network in juvenile myoclonic epilepsy. *Brain Behav* 2021;11:e2274
10. Wang Y, Berglund IS, Uppman M, Li TQ. Juvenile myoclonic epilepsy has hyper dynamic functional connectivity in the dorsolateral frontal cortex. *Neuroimage Clin* 2019;21:101604
11. Aerts HJ, Velazquez ER, Leijenaar RT, Parmar C, Grossmann P, Carvalho S, et al. Decoding tumour phenotype by noninvasive imaging using a quantitative radiomics approach. *Nat Commun* 2014;5:4006
12. Gillies RJ, Kinahan PE, Hricak H. Radiomics: images are more than pictures, they are data. *Radiology* 2016;278:563-577
13. Mo J, Liu Z, Sun K, Ma Y, Hu W, Zhang C, et al. Automated detection of hippocampal sclerosis using clinically empirical and radiomics features. *Epilepsia* 2019;60:2519-2529
14. Liu Z, Wang Y, Liu X, Du Y, Tang Z, Wang K, et al. Radiomics analysis allows for precise prediction of epilepsy in patients with low-grade gliomas. *Neuroimage Clin* 2018;19:271-278
15. Ségonne F, Dale AM, Busa E, Glessner M, Salat D, Hahn HK, et al. A hybrid approach to the skull stripping problem in MRI. *Neuroimage* 2004;22:1060-1075
16. Fischl B, Salat DH, Busa E, Albert M, Dieterich M, Haselgrove C, et al. Whole brain segmentation: automated labeling of neuroanatomical structures in the human brain. *Neuron* 2002;33:341-355
17. Ségonne F, Pacheco J, Fischl B. Geometrically accurate topology-correction of cortical surfaces using nonseparating loops. *IEEE Trans Med Imaging* 2007;26:518-529
18. Dale AM, Fischl B, Sereno MI. Cortical surface-based analysis. I. Segmentation and surface reconstruction. *Neuroimage* 1999;9:179-194
19. Focke NK, Diederich C, Helms G, Nitsche MA, Lerche H, Paulus W. Idiopathic-generalized epilepsy shows profound white matter diffusion-tensor imaging alterations. *Hum Brain Mapp* 2014;35:3332-3342
20. Ekmekci B, Bulut HT, Gümüştaş F, Yıldırım A, Kuştepe A. The relationship between white matter abnormalities and cognitive functions in new-onset juvenile myoclonic epilepsy. *Epilepsy Behav* 2016;62:166-170
21. Saini J, Sinha S, Bagepally BS, Ramchandraiah CT, Thennarasu K, Prasad C, et al. Subcortical structural abnormalities in juvenile myoclonic epilepsy (JME): MR volumetry and vertex based analysis. *Seizure* 2013;22:230-235
22. Zhong C, Liu R, Luo C, Jiang S, Dong L, Peng R, et al. Altered structural and functional connectivity of juvenile myoclonic epilepsy: an fMRI study. *Neural Plast* 2018;2018:7392187
23. Bartolini E, Pesaresi I, Fabbri S, Cecchi P, Giorgi FS, Sartucci F, et al. Abnormal response to photic stimulation in juvenile myoclonic epilepsy: an EEG-fMRI study. *Epilepsia* 2014;55:1038-1047
24. Ciumas C, Wahlin TB, Jucaite A, Lindstrom P, Halldin C, Savic

https://doi.org/10.3348/kjr.2022.0539

I. Reduced dopamine transporter binding in patients with juvenile myoclonic epilepsy. *Neurology* 2008;71:788-794
25. Rossi J, Cavallieri F, Giovannini G, Benuzzi F, Ballotta D, Vaudano AE, et al. Can disruption of basal ganglia-thalamocortical circuit in Wilson disease be associated with juvenile myoclonic epilepsy phenotype? *Brain Sci* 2022;12:553
26. Tae WS, Hong SB, Joo EY, Han SJ, Cho JW, Seo DW, et al. Structural brain abnormalities in juvenile myoclonic epilepsy patients: volumetry and voxel-based morphometry. *Korean J Radiol* 2006;7:162-172
27. Lin K, de Araujo Filho GM, Pascalicchio TF, Silva I, Tudesco IS, Guaranha MS, et al. Hippocampal atrophy and memory dysfunction in patients with juvenile myoclonic epilepsy. *Epilepsy Behav* 2013;29:247-251
28. Zhang J, Wu D, Yang H, Lu H, Ji Y, Liu H, et al. Correlations between structural brain abnormalities, cognition and electroclinical characteristics in patients with juvenile myoclonic epilepsy. *Front Neurol* 2022;13:883078
29. Mory SB, Betting LE, Fernandes PT, Lopes-Cendes I, Guerreiro MM, Guerreiro CA, et al. Structural abnormalities of the thalamus in juvenile myoclonic epilepsy. *Epilepsy Behav* 2011;21:407-411
30. Kim JH, Kim JB, Seo WK, Suh SI, Koh SB. Volumetric and shape analysis of thalamus in idiopathic generalized epilepsy. *J Neurol* 2013;260:1846-1854
31. Ur Özçelik E, Kurt E, Şirin NG, Eryürek K, Ulaşoglu Yıldız Ç, Harı E, et al. Functional connectivity disturbances of ascending reticular activating system and posterior thalamus in juvenile myoclonic epilepsy in relation with photosensitivity: a resting-state fMRI study. *Epilepsy Res* 2021;171:106569
32. O'Muircheartaigh J, Vollmar C, Barker GJ, Kumari V, Symms MR, Thompson P, et al. Focal structural changes and cognitive dysfunction in juvenile myoclonic epilepsy. *Neurology* 2011;76:34-40
33. Kim SH, Lim SC, Kim W, Kwon OH, Jeon S, Lee JM, et al. Extrafrontal structural changes in juvenile myoclonic epilepsy: a topographic analysis of combined structural and microstructural brain imaging. *Seizure* 2015;30:124-131
34. Gilsoul M, Grisar T, Delgado-Escueta AV, de Nijs L, Lakaye B. Subtle brain developmental abnormalities in the pathogenesis of juvenile myoclonic epilepsy. *Front Cell Neurosci* 2019;13:433
35. Gong J, Chang X, Jiang S, Klugah-Brown B, Tan S, Yao D, et al. Microstructural alterations of white matter in juvenile myoclonic epilepsy. *Epilepsy* Res 2017;135:1-8
36. van Griethuysen JJM, Fedorov A, Parmar C, Hosny A, Aucoin N, Narayan V, et al. Computational radiomics system to decode the radiographic phenotype. *Cancer Res* 2017;77:e104-e107
37. Lambin P, Leijenaar RTH, Deist TM, Peerlings J, de Jong EEC, van Timmeren J, et al. Radiomics: the bridge between medical imaging and personalized medicine. *Nat Rev Clin Oncol* 2017;14:749-762
38. Collins GS, Reitsma JB, Altman DG, Moons KG. Transparent reporting of a multivariable prediction model for individual prognosis or diagnosis (TRIPOD): the TRIPOD statement. *BMJ* 2015;350:g7594
39. Chawla NV, Bowyer KW, Hall LO, Kegelmeyer WP. SMOTE: synthetic minority over-sampling technique. *J Artif Intell Res* 2002;16:321-357
40. Lundberg SM, Lee SI. A unified approach to interpreting model predictions. proceedings.neurips.cc Web site. https://proceedings.neurips.cc/paper/2017/hash/8a20a8621978632d76c43dfd28b67767-Abstract.html. Accessed March 22, 2022
41. Geithner J, Schneider F, Wang Z, Berneiser J, Herzer R, Kessler C, et al. Predictors for long-term seizure outcome in juvenile myoclonic epilepsy: 25-63 years of follow-up. *Epilepsia* 2012;53:1379-1386
42. Betting LE, Mory SB, Li LM, Lopes-Cendes I, Guerreiro MM, Guerreiro CA, et al. Voxel-based morphometry in patients with idiopathic generalized epilepsies. *Neuroimage* 2006;32:498-502
43. Liu M, Concha L, Beaulieu C, Gross DW. Distinct white matter abnormalities in different idiopathic generalized epilepsy syndromes. *Epilepsia* 2011;52:2267-2275
44. Woermann FG, Free SL, Koepp MJ, Sisodiya SM, Duncan JS. Abnormal cerebral structure in juvenile myoclonic epilepsy demonstrated with voxel-based analysis of MRI. *Brain* 1999;122(Pt 11):2101-2108
45. Alhusaini S, Ronan L, Scanlon C, Whelan CD, Doherty CP, Delanty N, et al. Regional increase of cerebral cortex thickness in juvenile myoclonic epilepsy. *Epilepsia* 2013;54:e138-e141
46. Wandschneider B, Hong SJ, Bernhardt BC, Fadaie F, Vollmar C, Koepp MJ, et al. Developmental MRI markers cosegregate juvenile patients with myoclonic epilepsy and their healthy siblings. *Neurology* 2019;93:e1272-e1280
47. Kim JH, Suh SI, Park SY, Seo WK, Koh I, Koh SB, et al. Microstructural white matter abnormality and frontal cognitive dysfunctions in juvenile myoclonic epilepsy. *Epilepsia* 2012;53:1371-1378
48. Si X, Zhang X, Zhou Y, Sun Y, Jin W, Yin S, et al. Automated detection of juvenile myoclonic epilepsy using CNN based transfer learning in diffusion MRI. *Annu Int Conf IEEE Eng Med Biol Soc* 2020;2020:1679-1682
49. Johns MW. A new method for measuring daytime sleepiness: the Epworth sleepiness scale. *Sleep* 1991;14:540-545
50. Landvogt C, Buchholz HG, Bernedo V, Schreckenberger M, Werhahn KJ. Alteration of dopamine D2/D3 receptor binding in patients with juvenile myoclonic epilepsy. *Epilepsia* 2010;51:1699-1706
51. Lee HJ, Seo SA, Lee BI, Kim SE, Park KM. Thalamic nuclei volumes and network in juvenile myoclonic epilepsy. *Acta Neurol Scand* 2020;141:271-278
52. Renganathan R, Delanty N. Juvenile myoclonic epilepsy: under-appreciated and under-diagnosed. *Postgrad Med J* 2003;79:78-80